Phase contrast imaging measurements of reversed shear Alfvén eigenmodes during sawteeth in Alcator C-Moda)

E. M. Edlund, M. Porkolab, G. J. Kramer, L. Lin, Y. Lin, and S. J. Wukitch

Citation: Physics of Plasmas **16**, 056106 (2009); doi: 10.1063/1.3086869
View online: http://dx.doi.org/10.1063/1.3086869
View Table of Contents: http://scitation.aip.org/content/aip/journal/pop/16/5?ver=pdfcov
Published by the AIP Publishing

Articles you may be interested in

Validation of full-wave simulations for mode conversion of waves in the ion cyclotron range of frequencies with phase contrast imaging in Alcator C-Mod
Phys. Plasmas **22**, 082502 (2015); 10.1063/1.4927912

Measurements of ion cyclotron range of frequencies mode converted wave intensity with phase contrast imaging in Alcator C-Mod and comparison with full-wave simulations
Phys. Plasmas **19**, 082508 (2012); 10.1063/1.4745613

Deuterium beam acceleration with 3rd harmonic ion cyclotron resonance heating in Joint European Torus: Sawtooth stabilization and Alfvén eigenmodes
Phys. Plasmas **19**, 032115 (2012); 10.1063/1.3696858

Ion cyclotron range of frequency mode conversion physics in Alcator C-Mod: Experimental measurements and modelinga)
Phys. Plasmas **12**, 056104 (2005); 10.1063/1.1866142

Active and fast particle driven Alfvén eigenmodes in Alcator C-Moda)
Phys. Plasmas **12**, 056102 (2005); 10.1063/1.1865012

Reuse of AIP Publishing content is subject to the terms at: https://publishing.aip.org/authors/rights-and-permissions. Downloaded to IP: 198.125.176.142 On: Mon, 07 Mar 2016 18:31:12

Phase contrast imaging measurements of reversed shear Alfvén eigenmodes during sawteeth in Alcator C-Mod[a)]

E. M. Edlund,[1,b)] M. Porkolab,[1] G. J. Kramer,[2] L. Lin,[1] Y. Lin,[1] and S. J. Wukitch[1]
[1]*MIT Plasma Science and Fusion Center, Cambridge, Massachusetts 02139, USA*
[2]*Princeton Plasma Physics Laboratory, Princeton, New Jersey 08543, USA*

(Received 7 December 2008; accepted 30 January 2009; published online 23 March 2009)

Reversed shear Alfvén eigenmodes (RSAEs) have been observed with the phase contrast imaging diagnostic and Mirnov coils during the sawtooth cycle in Alcator C-mod [M. Greenwald *et al.*, Nucl. Fusion **45**, S109 (2005)] plasmas with minority ion-cyclotron resonance heating. Both down-chirping RSAEs and up-chirping RSAEs have been observed during the sawtooth cycle. Experimental measurements of the spatial structure of the RSAEs are compared to theoretical models based on the code NOVA [C. Z. Cheng and M. S. Chance, J. Comput. Phys. **71**, 124 (1987)] and used to derive constraints on the q profile. It is shown that the observed RSAEs can be understood by assuming a reversed shear q profile (up chirping) or a q profile with a local maximum (down chirping) with $q \approx 1$. © *2009 American Institute of Physics*. [DOI: 10.1063/1.3086869]

I. INTRODUCTION

The sawtooth crash in a tokamak plasma is a process whereby magnetic reconnection modifies the topology of the flux surfaces near the plasma core, inducing rapid energy and particle transport as well as causing redistribution of the current parallel to the magnetic field.[1–3] The sawtooth cycle is characterized by the abrupt crash in the central temperature, caused by the magnetic reconnection, followed by a relaxation and reheat phase during which the temperature increases nearly linearly in time and the parallel current density diffuses toward the core until an instability threshold is reached and another reconnection event occurs. After years of study there remain many questions as to the nature of both the physics of the magnetic reconnection and diffusion during the sawtooth cycle. In particular, there has been much debate over the evolution of the q profile (where $q \approx rB_\phi / R_0 B_\theta$ is the magnetic safety factor, r is the minor radial coordinate, B_ϕ is the toroidal magnetic field, R_0 is the tokamak major radius, and B_θ is the poloidal magnetic field), an important quantity in the stability of kink and interchange modes which may be responsible for initiating the reconnection process. While some studies have found that q_0, that is, q at the magnetic axis, remains well below unity throughout the sawtooth cycle,[3–5] others concluded that q_0 was close to or larger than unity following the crash, implying a complete reconnection process.[6–10] While the central temperature can increase by a factor of 2 or more during the relaxation process and can be readily measured by electron-cyclotron emission (ECE) diagnostics or Thomson scattering, the current density profile may change by only a few percent and is considerably more difficult to measure precisely. However, it is important for understanding the physics of the relaxation and reconnection processes that the evolution of the q profile be measured throughout the sawtooth cycle.

A particular class of Alfvénic instability, the reversed shear Alfvén eigenmode (RSAE, also Alfvén cascade) has proven very useful as a method of "magnetohydrodynamic (MHD) spectroscopy" for inferring the evolution of q in reversed shear equilibria (i.e., negative magnetic shear for some portion of the q profile near the plasma core), where the magnetic shear is defined as $s=(r/q)(dq/dr)$. The RSAE frequency is a strong function of the minimum value of q ($q_{\min}$) in equilibria with reversed shear.[11–13] Reversed shear q profiles are known to be present during the current ramp phase as the Ohmic current diffuses toward the core and is transiently peaked off axis, a fact confirmed by the observation of RSAEs in the presence of energetic ions,[13,14] motional Stark effect (MSE) measurements,[15,16] and numerical modeling.[17] When $q_{\min}$ is near an integer value the RSAEs appear in a characteristic "grand cascade" pattern whereby multiple modes chirp in frequency at rates proportional to their individual toroidal mode number. Comparison of the grand cascade pattern to the dispersion relationship provides a method by which the toroidal mode numbers can be identified and the value of $q_{\min}$ determined unambiguously.

Recent observations of RSAEs during the sawtooth cycle in Alcator C-Mod,[18] and also in the Joint European Torus (JET),[19,20] offer a method by which the evolution of the q profile during the sawtooth cycle can be studied to high precision. While Ref. 20 concluded that the up-chirping modes resembling RSAEs were incompatible with a reversed shear q profile based on analysis of the so-called tornado modes, it did not consider the possibility that a reversed shear q profile may exist transiently following the sawtooth crash in the giant sawteeth that were studied. In Alcator C-Mod the $q=1$ RSAEs are seen in plasmas at International Thermonuclear Experimental Reactor (ITER) relevant densities of $n_{e0} < 1.5 \times 10^{20}$ m^{-3} with ion-cyclotron resonance heating (ICRH) utilizing the on-axis fundamental hydrogen minority heating scheme at 80 MHz and 5.4 T in deuterium majority plasmas ($n_H/n_D \approx 0.05$). Importantly, the ICRH generates an energetic proton component with energies of approximately 100 keV or more, which provides the drive

[a)]Paper GI1 3, Bull. Am. Phys. Soc. **53**, 79 (2008).
[b)]Invited speaker.

 © 2009 American Institute of Physics

Reuse of AIP Publishing content is subject to the terms at: https://publishing.aip.org/authors/rights-and-permissions. Downloaded to IP: 198.125.176.142 On: Mon, 07 Mar 2016 18:31:12

for the Alfvén eigenmodes.[21] We find that the existence of the $q=1$ RSAEs requires a hollow current density profile interior to the sawtooth mixing radius. In this paper we present observations of $q=1$ RSAEs which indicate that during the relaxation process the q profile evolves from a state with a local maximum in q to a state with reversed shear, both of which are equivalent to a hollow current density profile. Models of the reconnection and reconnection processes are discussed in light of these observations.

The remainder of the paper is organized in three sections. Section II covers a brief discussion of the diagnostics followed by a presentation of representative observations of RSAEs during the sawtooth cycle. A commentary on the application of the RSAEs to models of the current relaxation is presented in Sec. III. Concluding remarks are given in Sec. IV.

II. OBSERVATIONS OF RSAES DURING THE SAWTOOTH CYCLE

Alcator C-mod is a compact, diverted tokamak operated at MIT with ITER relevant plasma parameters, such as density, magnetic field, safety factor, and shaping, and has a first wall covered with molybdenum tiles.[22] Representative plasma traces for experiments with RSAEs during sawteeth are shown in Fig. 1. The two primary diagnostics used in the Alcator C-Mod experiments for the study of the RSAEs are the phase contrast imaging (PCI) diagnostic[14] and the Mirnov coils. While the PCI diagnostic has proven to be very powerful due to its ability to detect perturbations from all flux surfaces it cannot provide a direct measure of the toroidal or poloidal mode numbers. When multiple RSAEs are present, as is the case where $q_{\min}$ is near an integer value, a set of mode numbers may be inferred by fitting the frequency spectra to the RSAE dispersion relationship. This method of indirect identification of the mode numbers is substantiated by direct measurement of the toroidal phase in cases where the RSAE amplitude was large enough to be detected by the Mirnov coils. The spatial information provided by the PCI diagnostic is used to extract additional constraints on the q profile through a synthetic diagnostic analysis. These methods and our main observations are described in the following.

A. Diagnostics

The PCI diagnostic is an internal reference beam interferometer using a 10.6 μm CO_2 laser beam expanded to a full width at half maximum power profile of approximately 14 cm. The detector is a 32 channel HgCdTe photoconductive array with a 3 dB point of approximately 10 MHz.[23] Signals for these experiments were digitized at 10 MHz. The output signal of the PCI system has an intensity proportional to the line integral of the electron density fluctuations along the beam path, that is, $I_{\mathrm{PCI}} \propto \int \tilde{n}_e dl$. The PCI system is calibrated through the detection of pressure perturbations in air in the range of 15–125 kHz. In the experiments presented here the system was optimized for large spatial coverage with each of the 32 channels corresponding to a radial extent of about 4.5 mm at the plasma midplane. Together, the 32 channel system provides measurements of the line-integrated spatial structure of the RSAEs. Interpretation of the signal is aided by comparison to a "synthetic diagnostic" which simulates the PCI system signals by numerically integrating density fluctuations and convolving with the system response function. This technique is described in Sec. II B.

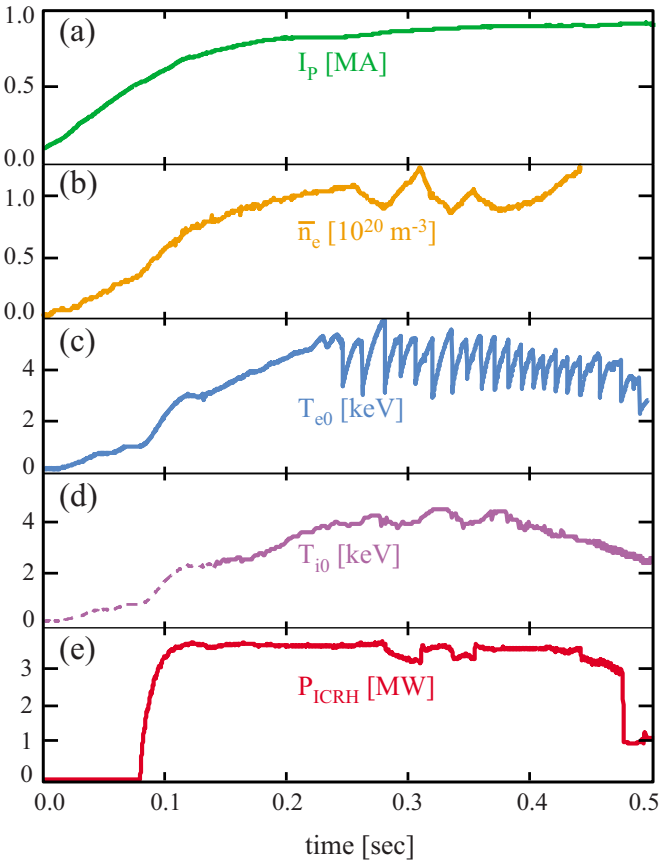

FIG. 1. (Color online) Experimental traces showing (a) total plasma current, (b) line-averaged electron density, (c) central electron temperature from the ECE diagnostic, (d) central deuterium ion temperature derived from the neutron flux, and (e) the injected ICRH power. The breaks in slope of the density trace, starting around 0.25 s, indicate transitions between L mode and ELM-free H mode. Ion temperature data are not available before 0.15 s and is represented as 0.8 times T_{e0} for this time range (dashed trace).

When the Doppler shift from toroidal rotation and the energetic particle β are negligible compared to the RSAE frequency and plasma β, an approximate dispersion relationship for the RSAEs (Ref. 12) can be put in the form

$$f_{\mathrm{RSAE}}^2 = f_0^2 + f_A^2\left(\frac{m}{q_{\min}(t)} - n\right)^2 + (\Delta f)^2, \tag{1}$$

where the first term (f_0) on the right hand side represents the effect of the geodesic-acoustic deformation of the Alfvén continuum, the second term (f_A) is the Alfvénic component, and the third term (Δf) represents small contributions to the frequency arising from the energetic ions and finite pressure gradients and is ignored in this analysis. In Eq. (1), $q_{\min}$ is the minimum value of q, and m and n are the poloidal and toroidal mode numbers, respectively. The acoustic component, arising from finite pressure, is to first order represented by the quantity

Reuse of AIP Publishing content is subject to the terms at: https://publishing.aip.org/authors/rights-and-permissions. Downloaded to IP: 198.125.176.142 On: Mon, 07 Mar 2016 18:31:12

$$f_0^2 = \frac{1}{(2\pi)^2}\frac{2T_e}{M_i R_0^2}\left(1+\frac{7}{4}\frac{T_i}{T_e}\right), \tag{2}$$

where T_e is the electron temperature, M_i is the ion mass, and R_0 is the tokamak major radius.[12] The Alfvénic frequency is given by the expression

$$f_A^2 = \frac{1}{(2\pi)^2}\frac{B^2}{R_0^2\mu_0\rho}, \tag{3}$$

where B is the modulus of the magnetic field and ρ is the mass density. While the temperature and density profiles are in general evolving in parallel with $q_{\min}$, in practice the time dependence is dominated by $q_{\min}(t)$ in the Alfvénic term. The temperature enters the dispersion relationship only through the f_0^2 term, which is dominant only when $k_\parallel \approx 0$ due to the relative magnitude of f_A^2 compared to f_0^2. The density enters the dispersion relation through f_A^2, but as shown in Ref. 3, the fractional change in density may be considerably smaller than the fractional change in q during the sawtooth cycle, and as the relevant quantity in the dispersion relationship is $\delta q \equiv m/n - q_{\min}$, we find that changes in q on the order of 10^{-3} can be equivalent to the effect from the change in density. Though this dispersion relationship was derived in the limit of large n and $q \gg 1$, it has been checked against numerical results from the ideal MHD code NOVA (Ref. 24) and found to be in agreement within about 5% for cases where $q_{\min} < 1$ and mode numbers of $n=2,3,4,5$. Equation (1) is valid when $q_{\min}$ is well away from the toroidicity-induced Alfvén eigenmode (TAE) value given by $q_{\mathrm{TAE}} = (m \pm 1/2)/n$. For reference, q_{TAE} for an $n=3$, $m=3$ mode is 0.83 which is significantly less than $q_{\min}$ inferred from the RSAEs, in the range of 0.92–0.97, depending on the conditions. The radial displacement eigenfunction of a RSAE is composed of a single dominant poloidal harmonic with weak sidebands of $m \pm 1$. The RSAEs exist near a maximum in the Alfvén continuum described by $\omega_A = k_\parallel V_A$, which is commonly associated with a minimum in the q profile which, when $q_{\min}$ decreases, produces the well known up-chirping RSAEs. During the sawtoothing phase it is expected that $q \approx 1$ in the plasma core which implies that $m=n$ for the dominant poloidal mode of the RSAE. Given this relation between m and n it is apparent from Eq. (1) that the rate at which the RSAE frequency increases due to a change in $q_{\min}$ is proportional to n, i.e., higher n RSAEs change frequency more quickly. This is the basis for the identification of the mode numbers from the frequency spectra measured by PCI and is illustrated in Fig. 2.

The Mirnov coils used in these experiments are positioned 10 cm below the geometric midplane at five toroidal locations. The large angle separation between coils allows for the identification of low n numbers with good accuracy. Frequency spectra from the PCI diagnostic and a Mirnov coil are presented in Fig. 2. The overlaid traces in the PCI spectrogram are a fit of the dispersion relationship [Eq. (1)] to the RSAE traces where the n numbers have been identified by the method outlined previously. The toroidal phase measurements for the observed modes have identified modes of $n=2-5$. This analysis is presented in Fig. 2(c) and confirms

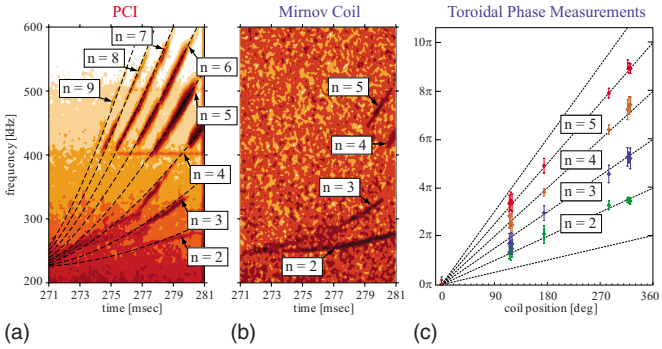

FIG. 2. (Color online) (a) Spectrogram of RSAEs excited during a sawtooth cycle as measured by PCI, with mode numbers inferred from the best fit to Eq. (1) overlaid in dashed line. (b) Spectrogram for the same time period measured by a Mirnov coil. (c) Measured phases of the modes detected by the Mirnov coils as a function of toroidal angle, confirming the inference from the PCI analysis.

the identification of the mode numbers by comparison of the PCI data to the dispersion relation [Eq. (1)], which will be used in the remainder of the paper for the cases where Mirnov data were not available.

B. Synthetic PCI analysis

A recent example of application of a synthetic PCI analysis for the study of short-wavelength electrostatic turbulence is reported in Ref. 25, and a similar procedure is followed here for analysis of Alfvén waves. The additional information supplied by the radial array of the 32-element PCI detector can be used to provide an additional constraint on the q profile. Given that the image of the perturbations created by PCI is a one-dimensional representation of an inherently two-dimensional structure, use of a synthetic diagnostic analysis is a necessity for interpreting the spatial information correctly. The measured signals suggest that the RSAE density perturbations are in general asymmetric about the magnetic axis and therefore an inversion of the PCI data is not possible without additional information. Rather, the RSAE density perturbation calculated by the ideal MHD code NOVA (Ref. 24) is used to construct a synthetic PCI diagnostic signal. In what follows, the q profiles used in the numerical analysis are constrained near the plasma edge ($r/a > 0.8$) by EFIT (Ref. 26) (which is based on edge magnetic measurements) and are determined in the core through profile scans with NOVA. In particular, comparing the measured frequency spectra of the RSAEs to Eq. (1) once the n numbers have been established allows for $q_{\min}(t)$ to be determined. The remainder of this paper will focus on the spatial structures of the RSAEs measured by PCI and the constraints on the q profile implied by these measurements.

The ideal MHD code NOVA solves for Alfvén eigenmodes in toroidal equilibrium using a nonvariational analysis. A standard output of NOVA is the two-dimensional fluid density perturbation in the poloidal plane. Taking $n_e \propto \rho$, where ρ is the fluid density, the fluid perturbation can be converted into an electron density perturbation which is then integrated along a viewing chord to produce a synthetic PCI signal. Numerical investigations of NOVA solutions for differ-

Reuse of AIP Publishing content is subject to the terms at: https://publishing.aip.org/authors/rights-and-permissions. Downloaded to IP: 198.125.176.142 On: Mon, 07 Mar 2016 18:31:12

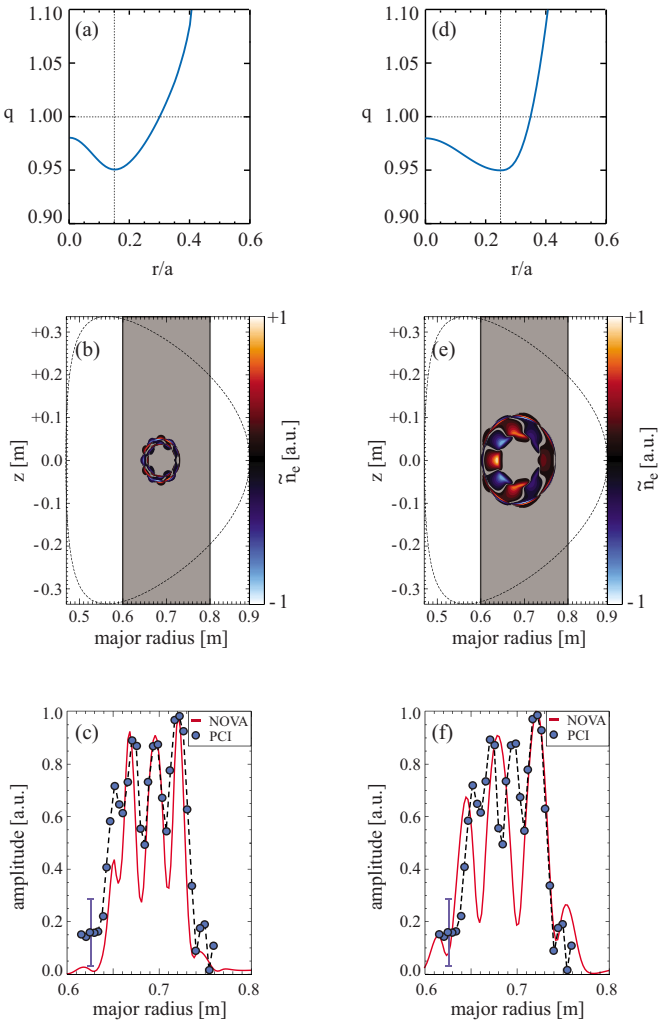

FIG. 3. (Color online) The synthetic PCI analysis shows the greatest sensitivity to r_{min}, which manifests as the peak spacing and width in the synthetic signal. (a) The input q profile with q_{min}=0.95, q_0=0.98, and r_{min}/a=0.15. (b) The two-dimensional density perturbation calculated by NOVA for an n=4 RSAE using the above q profile and (c) the resulting comparison between the experimental and synthetic PCI signals. Panels (d)–(f) use an unoptimized value of r_{min}/a=0.25 to illustrate the differences in synthetic diagnostic signal.

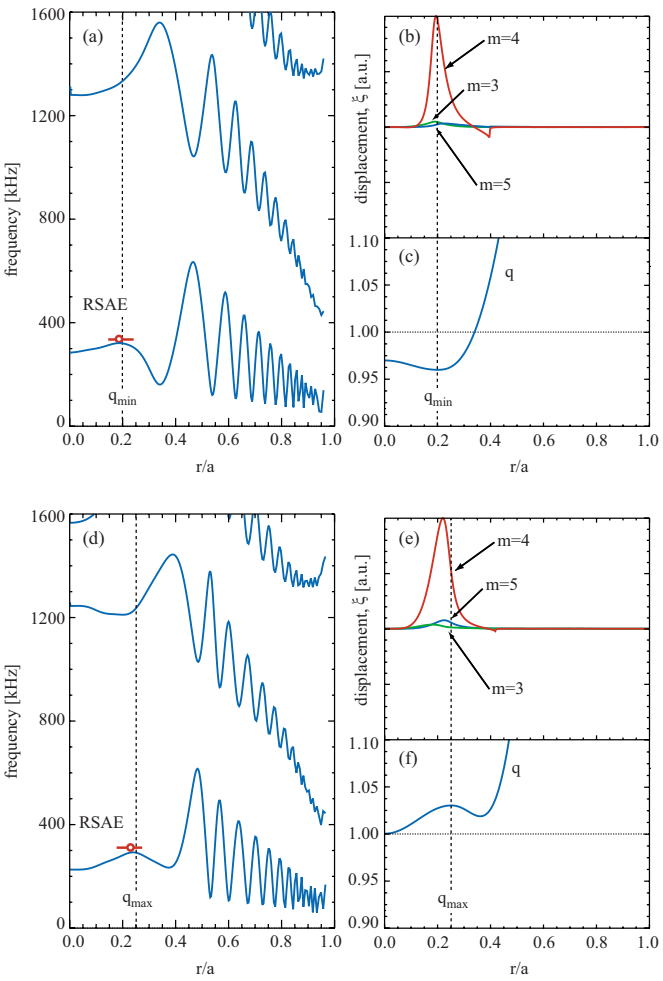

FIG. 4. (Color online) (a) Alfvén continuum plot from NOVA for an n=4 up-chirping RSAE. (b) The radial displacement eigenmode associated with the q profile shown in (c). Plots (d)–(f) pertain to a down-chirping RSAE for a q profile with a local maximum at r/a=0.25.

ent equilibria have shown that variation of the radial position of q_{min}, defined here as r_{min}, results in the strongest signature in the synthetic diagnostic analysis. Specifically, an increase in r_{min} translates to an increase in the peak spacing and peak width in the synthetic diagnostic signal. The q profiles of two equilibria are shown in Fig. 3, with the corresponding poloidal density perturbations and synthetic diagnostic comparison for an n=4 RSAE. The nodes in the line-integrated PCI signal structure arise from cancellation of positive and negative density perturbations along the beam path. Comparison of two synthetic diagnostic signals shows that the case with r_{min}/a=0.15 is in better agreement with the experimental PCI data than the case with r_{min}/a=0.25, though some discrepancy remains, particularly in the leftmost peak. The comparison between the experimental PCI data and synthetic PCI signal from the NOVA solutions can be quantified through the parameter $\chi^2=\Sigma_{i=1}^{32}(F_i^{PCI}-F_i^{syn})^2$, where F_i^{PCI} are the experimental PCI amplitudes, F_i^{syn} are the synthetic diagnostic amplitudes, and the sum is over the 32 radial positions of the PCI system. The best fit synthetic diagnostic solution is that which minimizes χ^2. There are two free parameters which can be varied to minimize the value of χ^2 for each synthetic diagnostic result. The first free parameter is the scaling of the synthetic diagnostic amplitude which is representative of the fact that NOVA calculates only relative density fluctuations. The second free parameter is the major radius of the reference position of the PCI array. At the time of these experiments the PCI system was only calibrated for channel spacing and not absolute position. To account for this uncertainty the experimental PCI data are collectively scanned in the major radius a few centimeters to minimize the value of χ^2.

C. RSAE constraints on the *q* profile

Two classes of RSAEs are observed during sawteeth. Most frequently, groups of up-chirping (increasing) frequency RSAEs are observed prior to the sawtooth crash. This class of RSAEs can be associated with a q profile with a minimum value less than unity. The second class of RSAEs is the down-chirping (decreasing) frequency branch. Interest-

Reuse of AIP Publishing content is subject to the terms at: https://publishing.aip.org/authors/rights-and-permissions. Downloaded to IP: 198.125.176.142 On: Mon, 07 Mar 2016 18:31:12

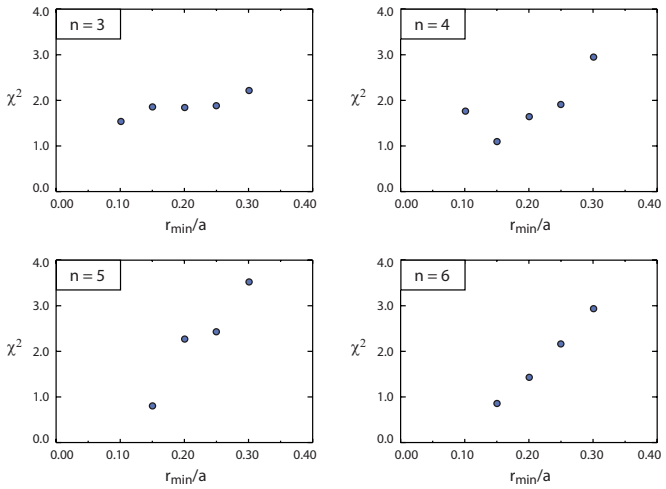

FIG. 5. (Color online) Plots of χ^2 as a function of $r_{\min}/a$ for the $n=3,4,5,6$ modes identified in Fig. 2 show a best fit solution near $r_{\min}/a=0.15$. No solutions at $r_{\min}/a=0.10$ were found for the $n=5$ and 6 cases.

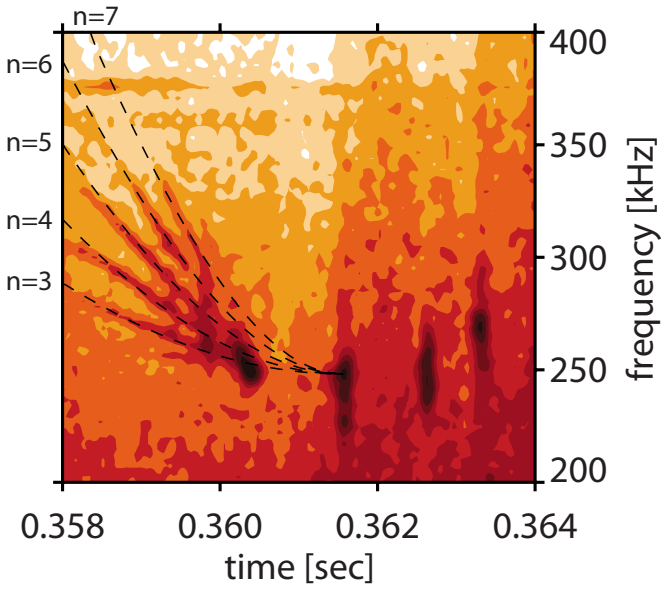

FIG. 6. (Color online) PCI spectrogram of down-chirping RSAEs immediately following a sawtooth crash. Toroidal mode numbers of $n=3-7$ are identified by comparison with Eq. (1) which implies that $q_{\max}\approx 1.03$ following the crash.

ingly this branch can be associated with a q profile with a local maximum above unity. Though often excited only weakly, sometimes such that the individual branches are hardly identifiable, their fairly regular presence suggests that q profiles with a local maximum may be a standard feature of the postcrash equilibrium. NOVA-K calculates both the down-chirping and up-chirping modes to be unstable in the presence of a energetic ion distribution based on experimental studies with the neutral particle analyzer in Alcator C-Mod.[27] It should be reiterated that the $q=1$ RSAEs observed during sawteeth are only observed in the low-density operating regime for Alcator C-Mod, and that we are unable to determine at this time if the RSAEs are absent in higher density plasmas because of the absence of reversed shear or because the energetic ion population is diminished in these conditions. Representative NOVA solutions of both classes of RSAEs are presented in Fig. 4. The up-chirping and down-chirping RSAEs will be examined separately in the following.

The up-chirping RSAEs are observed frequently in L-mode plasmas with 2–5 MW of ICRH and central electron densities in the range $(1.0–1.5)\times 10^{20}$ m^{-3}. They have also been observed in edge localized mode free (ELM-free) H-mode plasmas at comparable densities, though with lower amplitudes than in the L mode. A summary of the χ^2 values for the modes 3–6 shown from Fig. 2 as $r_{\min}$ is varied in the synthetic diagnostic analysis is shown in Fig. 5. The relatively flat distribution of points in the $n=3$ case is likely due a combination of comparatively lower signal to noise ratio in the experimental data and the tendency of the lower n NOVA solutions to have stronger distortion in the synthetic diagnostic analysis arising from interaction with the Alfvén continuum. This last effect arises because the width of the eigenmode scales inversely to m, the poloidal mode number. Thus, it is expected that the $n=3$, $m=3$ mode should be broader than the higher n modes, and consequently have a stronger interaction with the Alfvén continuum. That the synthetic diagnostic signal should be distorted by this effect is a consequence of $\tilde{n}_e\sim\nabla\cdot\vec{\xi}$, which becomes large at the point of interaction with the continuum due to the tendency of the eigenmode to be strongly peaked there. This may also explain the absence of the $n=1$ RSAE in all observations. Additionally, it should be noted that we have been unable to find NOVA solutions for the $n=5$ and $n=6$ cases for $r_{\min}/a<0.15$ and cannot definitively exclude the possibility of a best fit for these modes at lower values of $r_{\min}/a$. Taken together, this analysis suggests that $r_{\min}$ is near $r/a=0.15$. The dependence on the parameter q_0 is much weaker and we are exploring more carefully its influence on the synthetic PCI signals.

Though observed less frequently and generally with lower amplitudes, the down-chirping RSAEs are indicative of an equilibrium with $q\geq 1$ in the core. Following the sawtooth crash, the influence of the finite plasma resistivity will cause current to diffuse toward the axis and a state in approximate conformity with a $T_e^{3/2}$ profile. Thus, down-chirping RSAEs observed after the crash must be associated with a q profile that is decreasing, requiring $q>1$. Our studies with NOVA indicate that these down-chirping RSAEs are likely associated with a q profile with a local maximum near the core [illustrated in Figs. 4(d)–4(f)] rather than a more typical reversed shear profile. This is a result of the fact that a reversed shear q profile with $q>1$ produces an Alfvén continuum with a local minimum rather than a local maximum which assists RSAE formation. Figure 6 presents a case where the down-chirping RSAEs can be clearly identified as separate branches. In this case mode numbers of 3–7 are inferred from comparison with the dispersion relationship [Eq. (1)]. The results of the χ^2 calculations for the synthetic diagnostic analysis of these modes suggest that the local maximum is located in the region $0.25<r/a<0.30$.

Recent theoretical studies have shown that down-chirping RSAEs can also arise from kinetic effects[28] or from sufficiently large pressure gradients.[29] NOVA also contains

Reuse of AIP Publishing content is subject to the terms at: https://publishing.aip.org/authors/rights-and-permissions. Downloaded to IP: 198.125.176.142 On: Mon, 07 Mar 2016 18:31:12

RSAE solutions for reversed shear q profiles with $q>1$; however, their significant interaction with the Alfvén continuum suggests that they should be strongly damped. Analysis of the kinetic effects from Ref. 28 is needed to test whether these solutions can in fact be unstable. Given that a q profile with a local maximum near the core and $q>1$ yields unstable and relatively undamped RSAE solutions with the experimental profiles and is consistent with the PCI observations, we conclude that such a q profile may be present following the sawtooth crash. Furthermore, we will show that this type of q profile is consistent with modeling of the reconnection and relaxation phases of the sawtooth cycle discussed in the next section.

III. CONSTRAINED MODEL OF THE SAWTOOTH CYCLE

The presence of $q=1$ RSAEs offers the ability to constrain models of the current profile evolution during the sawtooth cycle. The following analysis illustrates how the RSAE constraints may be taken as a test of various models or used as a substitute for a free parameter, such as the Z_{eff} profile, in cases where it is not otherwise measured. The constraints provided by the observation of the RSAEs during the sawtooth cycle can be used for the purposes of constraining the reconnection process by requiring (1) that a q profile with a local maximum be produced from a state with a reversed shear and (2) that the relaxation process governing the diffusion of currents and electric fields reproduces the evolution from the state with the local maximum in q to a reversed shear q profile. Motivated by the conclusion that following the sawtooth crash $q>1$ (from the observation of the down-chirping RSAEs), it seems likely that a complete reconnection process occurs in these experiments and hence the reconnection may be well described by the Kadomtsev model,[30] though the absence of a direct measurement of q_0 prevents us from stating this with certainty. Numerical studies of the sawtooth cycle by Denton *et al.*[31] and Parail and Pereverzev[32] suggested that reversed shear q profiles can be generated during the sawtooth cycle and was used to explain the phenomenon of compound sawteeth, though their models used classical (Spitzer) resistivity which does not account for magnetically trapped particles which can significantly modify the plasma resistivity and consequent current diffusion. In the following we investigate the application of the Kadomtsev model to these cases and the relaxation process under classical and neoclassical resistivity models.

A. Implications of the Kadomtsev model

The Kadomtsev model describes two essentially separate features of the sawtooth crash: the constraints by which the topology is modified due to the reconnection event and the time scales under which the reconnection occurs. While the Kadomtsev model has been widely criticized for its inability to accurately predict the time scales for a range of machines and conditions, these criticisms do not necessarily invalidate the model of the topology modification. Within the Kadomtsev model the topology evolution during the reconnection is governed by the constraints (1) that the toroidal magnetic flux of the two reconnecting surfaces is conserved and (2) that surfaces of equal helical magnetic flux reconnect. The helical magnetic flux (Ψ^*) is the magnetic flux threading the surface defined by an $m=1$, $n=1$ instability which is assumed to be the driving force for the reconnection process. The functions Ψ^* and q are related by the equation

$$\Psi^*(r) = \alpha \int_0^r \left(\frac{1}{q(r')} - 1 \right) 2\pi r' dr', \tag{4}$$

where α is a normalization constant. Note that Eq. (4) can be inverted to find $q=q(\Psi^*)$. Following application of the reconnection model from the formerly described constraints, the postcrash helical flux function can be found and inverted to solve for the postcrash q profile. The reconnection process is illustrated by the arrows in the figure, showing the movement of a few representative surfaces from the initial (precrash) state to the final (postcrash) state. The Kadomtsev model can produce a local maximum in q, interestingly, only when the reconnection starts from a precrash state with reversed shear. In general, the magnitude of the peak in the postcrash q profile, that is, the value of $q_{\max}-q_0$, generated by this process increases with the value of $q_0-q_{\min}$ in the precrash state. In the model results shown in Fig. 7 the precrash $q_{\min}$ surface is at $r/a=0.25$, which gives rise to a postcrash local maximum at $r/a=0.35$. A postcrash state with $q_{\max}$ of about 1.03 is consistent with the down-chirping RSAE, and also in agreement with a precrash $q_{\min}$ of about 0.95 inferred from the up-chirping RSAEs. These results suggest that the postcrash q profiles generated by the Kadomtsev model may capture the gross features of the equilibrium inferred through observation of the RSAEs. These results are used as initial conditions in the modeling of the resistive relaxation process described in the next section.

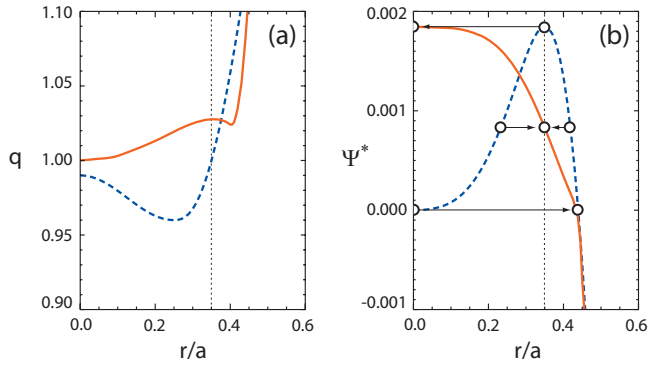

FIG. 7. (Color online) An example of the application of the Kadomtsev model. (a) The precrash q profile (blue dashed) with $q_{\min}=0.96$, $q_0=0.98$, and $r_{\min}/a=0.25$, and the postcrash q profile (orange solid) with a local maximum of $q_{\max}=1.03$ at $r_{\max}/a=0.35$. (b) The helical flux function before (blue dashed) and after (orange solid) the reconnection. The vertical dotted line indicates the precrash $q=1$ surface and the arrows indicate how the reconnection transforms the precrash state into the postcrash state.

B. Modeling the current density profile evolution

We now present a brief discussion of our attempts to model the relaxation process. The magnetic diffusion equation is derived from Maxwell's equations, ignoring the effect

Reuse of AIP Publishing content is subject to the terms at: https://publishing.aip.org/authors/rights-and-permissions. Downloaded to IP: 198.125.176.142 On: Mon, 07 Mar 2016 18:31:12

of the displacement current, and has a projection onto the parallel (to the magnetic field) direction given by

$$\frac{d}{dt}j_{\|} = \nabla^2 E_{\|} + O(E_{\perp}, j_{\perp}), \tag{5}$$

where $j_{\|}$ is the parallel current density, $E_{\|}$ is the parallel electric field, and the perpendicular current and electric field terms $(j_{\perp}, E_{\perp})$ are much smaller than the parallel terms and are dropped in this analysis. Formally, the bootstrap current should be considered as a component of $j_{\|}$; however, near the core the contribution of the bootstrap current may be ignorable on account of the small temperature and density gradients in this region. Ignoring the contributions of the bootstrap current allows for the use of the constitutive relation $E_{\|} = \eta_{\|} j_{\|}$, where $\eta_{\|} = g_{neo}\eta_0$ and g_{neo} contains the neoclassical corrections to the classical parallel resistivity, η_0. In our modeling we have used the neoclassical modifications from Sauter *et al.*[33] and initial conditions based on the previously described Kadomtsev model. The evolution of the temperature profiles is prescribed, based on experimental ECE data, a simplification over other models where the temperature profiles were evolved in parallel with the current.

Though the neoclassical corrections near the core may be small $(g_{neo} \approx 1)$ they can have a dramatic effect on the evolution of the q profile. The presence of the ∇^2 operator in the diffusion equation, acting on both the resistivity and the current density, causes Eq. (5) to be very sensitive to changes in profile shape. We have found that the neoclassical corrections from Sauter *et al.* induce a strong peaking of current at the magnetic axis, which can only be balanced by a strongly peaked impurity profile which tends to expel current from the core. Experimental measurement of high-Z impurities indicate that impurities such as Mo^{+31} and Mo^{+32} can have a nonzero derivative in the density profile at the magnetic axis,[34] suggesting that a peaked Z_{eff} profile may be a reasonable assumption for the model. Molybdenum can be a dominant impurity in Alcator C-Mod, which uses Mo tiles on the first wall, though at present we do not have Mo density profile measurements for these experiments. However, the robustness of the high-Z impurity peaking argument as an explanation for the generation of reversed shear with the neoclassical model is questionable, particularly in light of the observations of reversed shear during sawteeth in both DIII-D (Ref. 7) and JET (Ref. 19) which have carbon first walls. Two representative cases of the current modeling are presented in Fig. 8, where case (a) is the classical resistivity model with a flat impurity profile and case (b) is the neoclassical resistivity model with a peaked impurity profile. The impurity profiles used in this analysis are consistent with estimates of Z_{eff} from the loop voltage, though this does not provide any spatial information. In both cases the q profile evolves from the initial state to the final state with reversed shear, in general agreement with the observations of the RSAEs. These studies motivate the utility of core Z_{eff} profile measurements in conjunction with observation of $q=1$ RSAEs as a sensitive test of the neoclassical model near the magnetic axis.

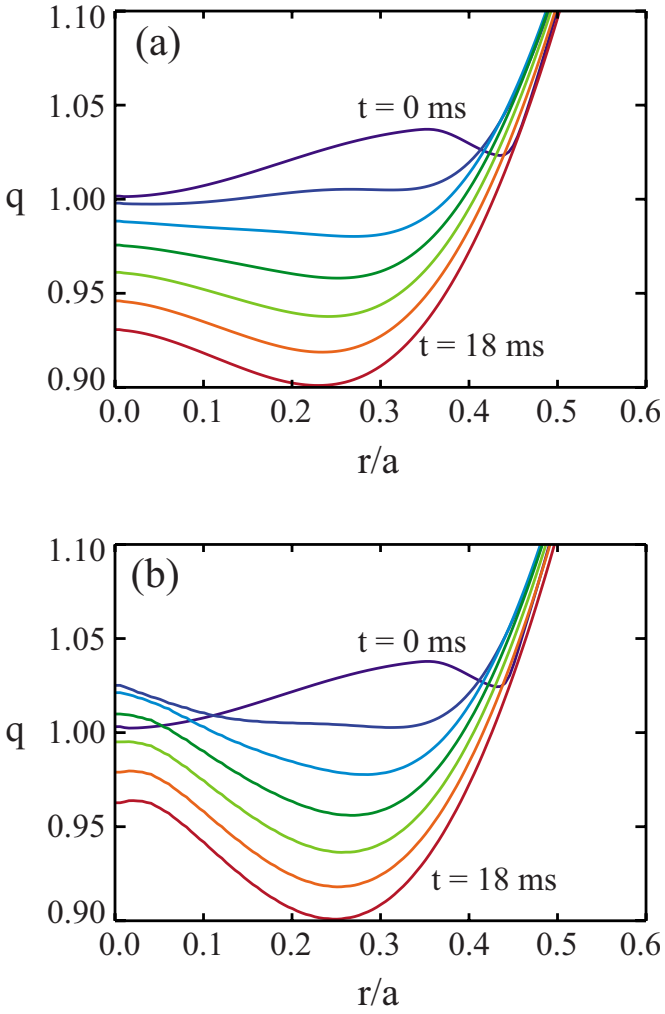

FIG. 8. (Color online) Evolution of q profiles during a sawtooth cycle of 18 ms at equal time intervals of 3 ms. The initial conditions are provided by the Kadomtsev model results similar to those presented in Fig. 7. The two cases are (a) classical resistivity with flat Z_{eff} profile and (b) neoclassical resistivity with peaked Z_{eff} profile.

IV. DISCUSSION AND SUMMARY

Strongly core localized RSAEs, with both up-chirping and down-chirping frequencies, have been observed in Alcator C-Mod with ICRF hydrogen minority heating in a deuterium majority plasma. The spatial and temporal measurements of the RSAEs provided by the PCI diagnostic provide constraints on the q profile through a comparison with the NOVA code. We find that $q_{\min}$ decreases to values in the range of 0.92–0.97 prior to the sawtooth crash. Analysis with NOVA has found $q=1$ RSAE solutions that agree with observations of the down-chirping and up-chirping RSAEs, both of which are calculated to be unstable in the presence of an ICRH generated energetic ion tail. The down-chirping RSAEs imply a peculiar q profile with a local maximum near $r/a=0.30$ following the sawtooth crash, while the up-chirping RSAEs imply a minimum in q located near $r/a=0.15$ prior to the sawtooth crash. The presence of RSAEs during the sawtooth cycle with ICRH, observed in Alcator C-Mod and JET plasmas, suggests that this phenomenon may be quite general.

Reuse of AIP Publishing content is subject to the terms at: https://publishing.aip.org/authors/rights-and-permissions. Downloaded to IP: 198.125.176.142 On: Mon, 07 Mar 2016 18:31:12

These results have the potential to provide valuable constraints for models of the sawtooth cycle, which may ultimately be developed to the point for use in predicting sawtooth behavior. At the present time, the analysis suffers from a lack of simultaneous impurity profile measurements. However, the observations of RSAEs implying a reversed shear q profile in the latter half of the sawtooth cycle can be used to bound this problem. That is, simulation of the current diffusion employing neoclassical resistivity requires a highly peaked impurity profile. The sharpness of the impurity profile near the magnetic axis may be decreased if there are additional physics that tend to move the neoclassical effects toward the classical limit. The presence of the down-chirping modes immediately following the sawtooth crash implies that $q>1$ and that a complete reconnection process has occurred in our experiments, though the absence of a measurement of q at the magnetic axis prevents us from determining this with absolute certainty. Our studies of the application of the Kadomtsev model to these equilibria show that a q profile with a local maximum can be reproduced only when the reconnection starts from a reversed shear q profile, and in this regard is consistent with the observation of the RSAEs.

ACKNOWLEDGMENTS

We would like to acknowledge the expert assistance of the Alcator C-Mod team in performing these experiments. We also acknowledge the valuable discussions with Jesus Ramos, Peter Catto, and Per Helander regarding our modeling and clarifications in regard to neoclassical theory.

This work is supported by the U.S. Department of Energy through Contract Nos. DE-FC02-99-ER54512 and DE-FC02-04ER54698.

[1] S. von Goeler, W. Stodiek, and N. Sauthoff, Phys. Rev. Lett. **33**, 1201 (1974).
[2] K. W. Gentle, M. E. Austin, and P. E. Phillips, Phys. Rev. Lett. **91**, 255001 (2003).
[3] H. Soltwisch, Rev. Sci. Instrum. **59**, 1599 (1988).
[4] M. F. Levinton, S. H. Batha, M. Yamada, and M. C. Zarnstorff, Phys. Fluids B **5**, 2554 (1993).
[5] R. C. Wolf, J. O'Rourke, A. W. Edwards, and M. von Hellermann, Nucl. Fusion **33**, 663 (1993).
[6] D. Wroblewski and R. T. Snider, Phys. Rev. Lett. **71**, 859 (1993).
[7] E. A. Lazarus, T. C. Luce, M. E. Austin, D. P. Brennan, K. H. Burrell, M. S. Chu, J. R. Ferron, A. W. Hyatt, R. J. Jayakumar, L. L. Lao, J. Lohr, M. A. Makowski, T. H. Osborne, C. C. Petty, P. A. Politzer, R. Prater, T. L. Rhodes, J. T. Scoville, W. M. Solomon, E. J. Strait, A. D. Turnbull, F. L. Waelbroeck, and C. Zhang, Phys. Plasmas **14**, 055701 (2007).
[8] A. Weller, A. D. Cheetham, A. W. Edwards, R. D. Gill, A. Gondhalekar, R. S. Granetz, J. Snipes, and J. A. Wesson, Phys. Rev. Lett. **59**, 2303 (1987).
[9] H. Weisen, G. Borg, B. Joye, A. J. Knight, and J. B. Lister, Phys. Rev. Lett. **62**, 434 (1989).
[10] G. J. Kramer, C. Z. Cheng, Y. Kusama, R. Nazikian, S. Takeji, and K. Tobita, Nucl. Fusion **41**, 1135 (2001).
[11] N. N. Gorelenkov, G. J. Kramer, and R. Nazikian, Plasma Phys. Controlled Fusion **48**, 1255 (2006).
[12] B. N. Breizman, M. S. Pekker, and S. E. Sharapov, Phys. Plasmas **12**, 1 (2005).
[13] S. E. Sharapov, B. Alper, H. L. Berk, D. N. Borba, B. N. Breizman, C. D. Challis, A. Fasoli, N. C. Hawkes, T. C. Hender, J. Mailloux, S. D. Pinches, and D. Testa, Phys. Plasmas **9**, 2027 (2002).
[14] M. Porkolab, C. Rost, N. Basse, J. Dorris, E. M. Edlund, L. Lin, Y. Lin, and S. J. Wukitch, IEEE Trans. Plasma Sci. **34**, 229 (2006).
[15] D. J. Kelliher, N. C. Hawkes, and P. J. McCarthy, Plasma Phys. Controlled Fusion **47**, 1459 (2005).
[16] B. W. Rice, T. S. Taylor, K. H. Burrell, T. A. Casper, C. B. Forest, H. Ikezi, L. L. Lao, E. A. Lazarus, M. E. Mauel, B. W. Stallard, and E. J. Strait, Plasma Phys. Controlled Fusion **38**, 869 (1996).
[17] M. Porkolab, R. Boivin, P. T. Bonoli, C. Fiore, M. Greenwald, A. Hubbard, I. H. Hutchinson, Y. In, E. Marmar, P. O'Shea, J. Ramos, J. Rice, J. C. Rost, J. A. Schachter, J. Snipes, Y. Takase, and S. M. Wolfe, *24th European Physical Society Conference on Controlled Fusion and Plasma Physics*, Berchtesgaden, Germany, 1997, edited by M. Schittenhelm, R. Bartiromo, and F. Wagner (The European Physical Society, Garching, 1997), Vol. 21A, Pt. II, p. 569.
[18] E. M. Edlund, M. Porkolab, G. J. Kramer, L. Lin, Y. Lin, and S. J. Wukitch, "Observation of reversed shear Alfvén eigenmodes during sawteeth in Alcator C-Mod," Phys. Rev. Lett. (accepted).
[19] S. E. Sharapov, B. Alper, Yu. F. Baranov, H. L. Berk, D. N. Borba, C. Boswell, B. N. Breizman, C. D. Challis, M. de Baar, P. de Vries, S. Hacquin, N. C. Hawkes, V. G. Kiptily, H. R. Koslowski, J. Mailloux, M. Nave, S. D. Pinches, P. Sandquist, and N. P. Young, *Proceedings of the 21st IAEA Conference*, Chengdu, China, 2006 (International Atomic Energy Agency, Vienna, 2007), Vol. IAEA-CN-149, p. EX/P6–EX/P19.
[20] P. Sandquist, S. E. Sharapov, M. Lisak, and T. Johnson, Phys. Plasmas **14**, 122506 (2007).
[21] M. N. Rosenbluth and P. H. Rutherford, Phys. Rev. Lett. **34**, 1428 (1975).
[22] M. Greenwald, D. Andelin, N. Basse, S. Bernabei, P. Bonoli, B. Bose, C. Boswell, R. Bravenec, B. Carreras, I. Czeigler, E. Edlund, D. Ernst, A. Fasoli, M. Ferrara, C. Fiore, R. Granetz, O. Grulke, T. Hender, J. Hosea, D. H. Howell, A. Hubbard, J. Hughes, I. Hutchinson, A. Ince-Cushman, J. Irby, B. LaBombard, R. LaHaye, L. Lin, Y. Lin, B. Lipschultz, J. Liptac, S. Lisgo, A. Lynn, E. Marmar, K. Marr, D. R. Mikkelsen, R. McDermott, D. Mossessian, A. Parisot, R. Parker, C. Phillips, P. Phillips, M. Porkolab, M. Redi, J. Rice, W. Rowan, M. Sampsell, G. Schilling, S. Scott, J. T. Scoville, N. Smick, J. Snipes, P. Stangby, V. Tang, J. Terry, M. Ulrickson, G. Wallace, D. Whyte, J. Wilson, J. Wright, S. Wolfe, S. Wukitch, B. Youngblood, H. Yuh, K. Zhurovich, and S. Zweben, Nucl. Fusion **45**, S109 (2005).
[23] A. Mazurenko, Ph.D. thesis, MIT, 2001.
[24] C. Z. Cheng and M. S. Chance, J. Comput. Phys. **71**, 124 (1987).
[25] L. Lin, M. Porkolab, E. M. Edlund, C. J. Rost, C. L. Fiore, M. Greenwald, Y. Lin, D. R. Mikkelsen, N. Tsujii, and S. J. Wukitch, Phys. Plasmas **16**, 012502 (2009).
[26] L. L. Lao, H. St. John, R. D. Stambaugh, A. G. Kellman, and W. Pfeiffer, Nucl. Fusion **25**, 1611 (1985).
[27] V. Tang, R. R. Parker, P. T. Bonoli, J. C. Wright, R. S. Granetz, R. W. Harvey, E. F. Jaeger, J. Liptac, C. L. Fiore, M. Greenwald, J. H. Irby, Y. Lin, and S. J. Wukitch, Plasma Phys. Controlled Fusion **49**, 873 (2007).
[28] N. N. Gorelenkov, Phys. Plasmas **15**, 110701 (2008).
[29] G. J. Kramer, N. N. Gorelenkov, R. Nazikian, and C. Z. Cheng, Plasma Phys. Controlled Fusion **46**, L23 (2004).
[30] B. B. Kadomtsev, Sov. J. Plasma Phys. **1**, 389 (1975).
[31] R. E. Denton, J. F. Drake, R. G. Kleva, and D. A. Boyd, Phys. Rev. Lett. **56**, 2477 (1986).
[32] V. V. Parail and G. V. Pereverzev, Sov. J. Plasma Phys. **6**, 14 (1980).
[33] O. Sauter, C. Angioni, and Y. R. Lin-Liu, Phys. Plasmas **6**, 2834 (1999).
[34] D. Pacella, L. Gabellieri, G. Mazzitelli, K. B. Fournier, and M. Finkenthal, Plasma Phys. Controlled Fusion **39**, 1501 (1997).

Reuse of AIP Publishing content is subject to the terms at: https://publishing.aip.org/authors/rights-and-permissions. Downloaded to IP: 198.125.176.142 On: Mon, 07 Mar 2016 18:31:12